

1

2           **A physically-based model for dissolved pollutant**  
3           **transport over impervious surfaces**

4           Taotao Zhang<sup>a,b, c</sup>, Yang Xiao<sup>a, b</sup>, Dongfang Liang<sup>d</sup>, Hongwu Tang<sup>a, b</sup>,  
5                           Junzeng Xu<sup>a, c</sup>, Saiyu Yuan<sup>a, b</sup>, Bin Luan<sup>b</sup>

6

7           <sup>a</sup> State Key Laboratory of Hydrology-Water Resources and Hydraulic Engineering, Hohai  
8           University, Nanjing 210098, China

9           <sup>b</sup> College of Water Conservancy and Hydropower Engineering, Hohai University, Nanjing 210098,  
10           China

11           <sup>c</sup> College of Agricultural Engineering, Hohai University, Nanjing 210098, China

12           <sup>d</sup> Department of Engineering, University of Cambridge, Cambridge CB2 1PZ, UK

13

14           **Corresponding author:** Yang Xiao, E-mail address: [sediment\\_lab@hhu.edu.cn](mailto:sediment_lab@hhu.edu.cn)

15

16

17 **Abstract:**

18 Dissolved pollutant transport over the ground surface is one of the main contributors  
19 to water pollution in urban environment. However, existing widely applied transport  
20 models are semi-empirical and the mechanism of the dissolved pollutant runoff is still  
21 not well understood. A novel physically-based transport model for dissolved pollutant  
22 is herein proposed by adopting a “control layer” concept in the overland flow. This  
23 transport model assumes that the dissolved pollutant in the upper runoff water is  
24 completely mixed with that in the underneath control layer. To verify the proposed  
25 model, a series of laboratory experiments were conducted. It showed that the  
26 predictions made by the model are in good agreement with the experimental results.  
27 The depth of the control layer is mainly correlated with the bed slope and shows no  
28 obvious dependence on rainfall intensity. The minimum depth of the control layer is  
29 bounded by a limiting value. In addition, the maximum pollutant transport rate is  
30 found to occur at the time of concentration. The rainfall intensity, bed slope, surface  
31 roughness and catchment length are dominant factors that control the dissolved  
32 pollutant transport. The wash-off coefficient is a function of time and is found to be  
33 the reciprocal of the average water depth of the catchment area over which the  
34 equilibrium state has been reached. This study advances the understanding of the  
35 mechanism of the dissolved pollutant transport in urban environment.

36

37 **Keywords:** Dissolved pollutant; Rainfall simulation; Wash-off coefficient; Rainfall  
38 runoff; Transportation of pollutants.

## 39 **1 Introduction**

40 Pollutants originating from urban impervious surfaces, such as roads and squares,  
41 have been recognized as a major contributor to the deterioration of water quality  
42 (Brezonik and Stadelmann, 2002; Angela et al., 2019; Lee and Bang, 2000; Vaze and  
43 Chiew, 2002). It has been predicted that 64% of the “developing world” and 86% of  
44 the “developed world” will be urbanized by 2050 (Montgomery, 2008). The ongoing  
45 urbanization will inevitably further exacerbate the urban storm water pollution (Wang  
46 et al., 2013). In this context, understanding the mechanism of pollutant transport on  
47 impervious surfaces is essential for developing more advanced pollution management  
48 strategies (Hong et al., 2016).

49 Among the various substances that make up of urban stormwater pollutants, solid  
50 particles are widely considered as a major cause of contamination in receiving water  
51 (Fletcher et al., 2013). Most of the stormwater-generated pollutants are deemed to be  
52 adsorbed onto solid particles, especially the fine particles (Sartor and Boyd, 1974;  
53 Sheng et al., 2008). Therefore, most of the existing studies have focused on the  
54 particulate matter transport process by stormwater, and a number of transport models  
55 have been developed in the past (Metcalf and Eddy Inc, 1971; Sartor and Boyd, 1974;  
56 Alley, 1981; Charbeneau and Barrett, 1998; Irish et al., 1998; Osuch-Pajdzińska and  
57 Zawilski, 1998; Deletic et al., 2000; Kim et al., 2005; Shaw et al., 2006; Egodawatta  
58 et al., 2007, 2009; Massoudieh et al., 2008; Hong et al., 2016; Muthusamy et al.,  
59 2018). Many transport models were based on the assumption that the rate of pollutant  
60 transport from an effectively impervious surface is directly proportional to the mass of

61 the remaining pollutant (Metcalf and Eddy Inc, 1971; Sartor and Boyd, 1974;  
62 Charbeneau and Barrett, 1998; Egodawatta et al., 2007, 2009; Muthusamy et al.,  
63 2018). In the earlier studies, the exponential transport model has thus been widely  
64 applied to the particulate pollutant transport process over impervious surfaces.

65 In practice, stormwater-borne pollutants can also appear in the dissolved phase as  
66 well as in the particulate phase (Sheng et al., 2008; Hong et al., 2017). The  
67 contribution from the dissolved pollutants to water pollution can be significant  
68 (Miguntanna et al., 2013). Goonetilleke et al. (2005) indicated that much of the  
69 pollutants transported were in the dissolved form and the common management  
70 technique of targeting particulate pollutants in urban stormwater quality control could  
71 have only limited efficiency. The difference in the transport of dissolved and  
72 particulate pollutants can be largely due to their different physical and chemical  
73 properties. Gauta et al. (2019) noted that the accuracy of the exponential transport  
74 model was clearly best for particulate pollutants, but might not be appropriate for  
75 dissolved pollutants. Xiao et al. (2016, 2017) conducted a series of experiments to  
76 investigate the transport process of dissolved pollutants over impervious surfaces, and  
77 a mathematical transport model was developed by combining the analytical equations  
78 for overland flows and the exponential equation for the pollutant wash-off. They  
79 suggested that both dissolved and particulate pollutants obey the exponential transport  
80 law. The difference in the transport of dissolved and particulate pollutants can be  
81 significant, which is reflected in the value of the wash-off coefficient  $k$ . The  
82 wash-off coefficient  $k$ , with units  $m^{-1}$ , is a key parameter for the exponential

83 transport model (Alley, 1981; Egodawatta et al., 2007; Soonthornnonda et al., 2008).  
84 The value of  $k$  may vary with the rainfall intensity, pollutant type and the physical  
85 characteristics of the catchment (Alley, 1981; Millar, 1999). Although the exponential  
86 equation has been widely used in many water quality models, such as the SWMM  
87 model, it still belongs to a class of semi-empirical models as the wash-off coefficient  
88  $k$  is an empirical parameter with no direct physical meaning (Egodawatta et al.,  
89 2007). However, for the dissolved pollutant, Zhang et al. (2018) suggested that the  
90 wash-off coefficient  $k$  may be related to the water depth and thus be assigned a  
91 physical meaning. Their study focused on the solute transport over vegetated  
92 impervious surfaces, and the idea of the “stationary water layer” was proposed  
93 according to the experimental results. In this study, the “stationary water layer” theory  
94 will be extended to describe the mechanism of dissolved pollutant transport over  
95 impervious surfaces.

96 Our objective is to develop and validate a novel physically-based model for  
97 predicting the transport process of dissolved pollutants over impervious surfaces,  
98 which may help advance our understanding of stormwater wash-off phenomena. To  
99 achieve this, the “stationary water layer” theory (Zhang et al., 2018) is coupled with  
100 the analytical equations for overland flows (Stephenson and Meadows, 1986). To  
101 validate the newly established model, a series of laboratory experiments, involving  
102 different rainfall intensities and bed slopes, have been conducted using rainfall  
103 simulators over uniform-sloped idealized rectangular catchments.

104

## 105 2 Mathematical model

106 In this study, only uniform and steady rainfall events are considered. For a  
107 uniform and steady rainfall distributed over a rectangular homogeneous impervious  
108 catchment with a uniform slope, an analytical solution to the kinematic wave equation  
109 has been derived by Stephenson and Meadows (1986). The analytical solution can be  
110 described as follows:

$$111 \quad t_c = \left[ L / (\alpha I^{m-1}) \right]^{1/m} \quad (1)$$

$$112 \quad q_t = \alpha (h)^m = \alpha (It)^m, \quad 0 \leq t \leq t_c \quad (2)$$

$$113 \quad q_t = \alpha (h)^m = \alpha (It_c)^m = LI, \quad t_c \leq t \leq T \quad (3)$$

$$114 \quad q_t = LI - I^m \alpha^{1/m} q_t^{1-1/m} (t - T), \quad T \leq t \quad (4)$$

$$115 \quad Q_t = q_t B \quad (5)$$

116 where,  $t$  is the time (s);  $t_c$  is the time of concentration (s);  $T$  is the rainfall  
117 duration (s);  $I$  is the rainfall intensity (m/s);  $L$  is the length of the watershed (m);  
118  $B$  is the width of the watershed (m);  $q_t$  is the discharge per unit width which is  
119 equal to the product of velocity and water depth (m<sup>2</sup>/s);  $Q_t$  is the flow rate (m<sup>3</sup>/s);  
120  $h$  is the water depth (m);  $\alpha$  and  $m$  are two coefficients which can be derived  
121 from the Manning equation as follows.

$$122 \quad \alpha = S_0^{1/2} / n; \quad m = 5/3 \quad (6)$$

123 where  $n$  is the Manning roughness coefficient and  $S_0$  is the bed slope.

124 The time needed to reach the equilibrium outflow rate at the end of the catchment  
125 is referred to as the time of concentration ( $t_c$ ), which can be roughly taken as the time  
126 required for a raindrop to move from the top of the slope to the outlet (Liang et al.,

127 2015). At the equilibrium stage, the constant maximum runoff rate can be calculated  
 128 as:

$$129 \quad Q_{\max} = LBI \quad (7)$$

130 where  $Q_{\max}$  is the maximum or equilibrium flow rate ( $\text{m}^3/\text{s}$ ).

131 According to Zhang et al. (2018), some logical assumptions can be made  
 132 regarding the rainfall-runoff process: (a) it takes the time  $t_{cx}$  for the flow at a  
 133 location  $x$  on the catchment to reach the equilibrium state, after which the flow at  
 134 this location remains constant; and (b) the flow is uniform with a constant water depth,  
 135 flow rate  $Q(x,t)$  and velocity  $v(x,t)$  downstream of the location  $x$  at time  $t_{cx}$ .

136 Under these assumptions, the values of  $v(x,t)$  and  $Q(x,t)$  can be derived as:

$$137 \quad v(x,t) = \frac{dx}{dt} = \frac{dQ(x,t)}{BI dt}, \quad \mathbf{0} \leq t \leq t_{cx} \quad (8)$$

$$138 \quad v(x,t) = v(x,t_{cx}), \quad t_{cx} \leq t \quad (9)$$

$$139 \quad v(x+a,t_{cx}) = v(x,t_{cx}), \quad \mathbf{0} \leq a \leq L - x \quad (10)$$

$$140 \quad Q(x+a,t_{cx}) = Q(x,t_{cx}) = xBI, \quad \mathbf{0} \leq a \leq L - x \quad (11)$$

141 According to Eqs. (1) and (6), the formulation of  $t_{cx}$  can be written as:

$$142 \quad t_{cx} = \left[ x / (\alpha I^{m-1}) \right]^{1/m} = \left[ x / (\alpha I^{2/3}) \right]^{3/5} \quad (12)$$

143 Combining Eqs. (2), (5), (6), and (8), we can obtain the formulation for  $v(x,t)$ :

$$144 \quad v(x,t) = \frac{5}{3} \alpha (It)^{2/3}, \quad \mathbf{0} \leq t \leq t_{cx} \quad (13)$$

145 In studying the transport of solute on soil slopes, many previous researchers  
 146 (Ahuja et al., 1981; Gao et al., 2004, 2005; Deng et al., 2005) suggested that a “thin  
 147 layer” (the so-called mixing layer, exchange layer or active layer) near the soil surface

148 controls the transfer of pollutants between the soil slope and the overland flow. As for  
149 vegetated surfaces, Zhang et al. (2018) suggested that the rainwater accumulates in  
150 the catchment to form a thin stationary water layer at the onset of the rainfall.  
151 Meanwhile, the pollutant begins to dissolve in this stationary water layer. After the  
152 beginning of overland flow, the pollutant in the stationary water layer gets gradually  
153 diffused into the upper runoff layer and then flows out of the catchment. Similarly, we  
154 assume that there is a thin water layer dominating the dissolved pollutant transport  
155 over impervious surfaces. We define this thin water layer as the “control layer”. For  
156 an homogeneous catchment, the depth of this control layer at a location is regarded to  
157 be a constant. At the beginning of overland flow ( $t = 0$ ), the depth of the control  
158 layer is defined as  $h_0$  (m). Compared with the soil slope and vegetated surface, the  
159 impervious surface allows the more rapid mixing of the water in the control layer with  
160 the upper runoff water. Hence, the mixing layer theory (Ahuja et al., 1981) can be  
161 applied to the control layer. Applying the mixing layer theory, we assume that  
162 pollutant concentration in the upper runoff water is equal to that in the underlying  
163 water in the control layer.

164 As in many previous studies (Gao et al., 2004, 2005; Deng et al., 2005; Kim et  
165 al., 2005; Muthusamy et al., 2018), the dissolved pollutant is assumed to be uniformly  
166 distributed on the catchment surface before the start of rainfall. Hence, the initial  
167 pollutant concentration can be calculated to be:

$$168 \quad C_0 = \frac{W_0}{BLh_0} = \frac{W_0}{Ah_0} \quad (14)$$

169 where  $C_0$  is the initial runoff pollutant concentration (g/L);  $W_0$  is the initial mass



170 of pollutant on the surface (kg); and  $A$  is the area of catchment ( $\text{m}^2$ ).

171 The water depth  $h$  along the catchment can be expressed as follows:

172 
$$h(x, t) = h_0 + It, \quad \mathbf{0} \leq t \leq t_{cx} \quad (15)$$

173 
$$h(x, t) = h_0 + It_{cx}, \quad t_{cx} < t \quad (16)$$

174 At time  $t$  ( $\mathbf{0} \leq t \leq t_c$ ), the raindrops move from the top edge of the catchment to

175 location  $x$ . According to Eq. (13), the value of  $x$  can be calculated as follows:

176 
$$x = \int_0^t v(x, t) dt = \int_0^t \frac{5}{3} \alpha (It)^{2/3} dt = \alpha I^{2/3} t^{5/3} \quad (17)$$

177 According to Eq. (11), the runoff rates from the top boundary of the catchment,

178  $x = \mathbf{0}$ , to  $x$  have reached the equilibrium state and the runoff rates from  $x$  to the

179 bottom of the catchment  $x=L$  are equal to the runoff rate at location  $x$ . From the

180 analysis of Zhang et al. (2018), the amount of water and pollutant flowing out of the

181 catchment at  $t$  ( $\mathbf{0} \leq t \leq t_c$ ) depends only on the processes taking place in the

182 catchment upstream of  $x$ . When the raindrops move from the top edge of the

183 catchment to  $x$ , the pollutant is also transported to  $x$ . Taking into account the effect

184 of diffusion, we assume that the pollutant concentration from 0 to  $x$  is uniform at

185 the time of  $t_{cx}$ . The total water volume from 0 to  $x$  at time  $t$  can be calculated to

186 be:

187 
$$V(x, t) = \int_0^x Bh(x, t) dx = B\alpha I^{2/3} t^{5/3} \left( h_0 + \frac{5}{8} It \right) \quad (18)$$

188 The pollutant concentration at the outlet at time  $t$  is defined as  $C_t$  (g/L).

189 According to the above hypothesis, the pollutant concentration from 0 to  $x$  is equal

190 to  $C_t$ . During a tiny interval of  $\Delta t$ , the runoff moves forward by a small distance of

191  $\Delta x$  :

$$192 \quad \Delta x = v(x, t) \Delta t = \frac{5}{3} \alpha (It)^{2/3} \Delta t \quad (19)$$

193 It means that over the area from 0 to  $x+\Delta x$  the runoff has reached an equilibrium  
194 state. We define the increase in the pollutant concentration as  $\Delta C_i$  (g/L) during  $\Delta t$  .

195 In this small duration of  $\Delta t$  , from Eq. (17), the volume of rainfall input from 0 to  
196  $x+\Delta x$  can be calculated by:

$$197 \quad V_{rain} = (x + \Delta x) BI \Delta t = B\alpha I^{5/3} (t + \Delta t)^{5/3} \Delta t \quad (20)$$

198 The increase in the amount of pollutant  $\Delta W$  can be expressed as follows.

$$199 \quad \Delta W = \frac{\Delta x W_0}{L} = \frac{5W_0}{3L} \alpha (It)^{2/3} \Delta t \quad (21)$$

200 According to the law of conservation of mass of the solute, we can obtain the  
201 following equation during the period from  $t$  to  $t + \Delta t$  .

$$202 \quad C_i V(x, t) + \Delta W = (C_i + \Delta C_i) (V(x + \Delta x, t + \Delta t) + V_{rain}) \quad (22)$$

203 Combining Eqs. (18), (19), (20), (21), and (22), we obtain:

$$204 \quad C_i B \alpha h_0 I^{2/3} t^{5/3} + \frac{5}{8} C_i B \alpha I^{5/3} t^{8/3} + \frac{5W_0}{3L} \alpha (It)^{2/3} \Delta t = C_i B \alpha h_0 I^{2/3} (t + \Delta t)^{5/3} + \\ \frac{5}{8} C_i B \alpha I^{5/3} (t + \Delta t)^{8/3} + \Delta C_i B \alpha h_0 I^{2/3} (t + \Delta t)^{5/3} + \frac{5}{8} \Delta C_i B \alpha I^{5/3} (t + \Delta t)^{8/3} + \\ C_i B \alpha I^{5/3} (t + \Delta t)^{5/3} \Delta t + \Delta C_i B \alpha I^{5/3} (t + \Delta t)^{5/3} \Delta t \quad (23)$$

206 In the above Eq. (23), the terms of  $(t + \Delta t)^{5/3}$  and  $(t + \Delta t)^{8/3}$  can be approximated  
207 using the first order Taylor expansion:

$$208 \quad (t + \Delta t)^{5/3} = t^{5/3} + \frac{5}{3} t^{2/3} \Delta t + R_1(\Delta t) \quad (24)$$

209 
$$(t + \Delta t)^{8/3} = t^{8/3} + \frac{8}{3} t^{5/3} \Delta t + R_1(\Delta t) \quad (25)$$

210 where  $R_1(\Delta t)$  represents the higher-order small terms. Combining Eqs. (23), (24),  
 211 and (25) and neglecting the second order small terms, Eq. (23) can be converted into a  
 212 differential equation.

213 
$$\frac{dC_t}{dt} = -C_t \frac{5h_0 + 8It}{3t(h_0 + 5It/8)} + \frac{5W_0}{3At(h_0 + 5It/8)} \quad (26)$$

214 Unfortunately, there is no analytical solution to the above differential equation.  
 215 Hence, the modified Euler method with second order accuracy is used to solve the  
 216 above differential equation. This modified Euler method consists of a predictor step  
 217 and a corrector step in each time advancement:

Predictor step: 
$$C^p = C_t + \Delta t \frac{dC_t}{dt} \quad (27)$$

Corrector step: 
$$C^c = C_t + \Delta t \frac{dC^p}{dt} \quad (28)$$

$$C_{t+\Delta t} = \frac{C^c + C^p}{2} \quad (29)$$

218 where  $p$  and  $c$  denote the predictor and corrector steps respectively,  $\Delta t$  is the time  
 219 step. The initial pollutant concentration ( $t = 0$ ) can be calculated by Eq. (14). The  
 220 values of subsequent concentrations can then be obtained successively once the given  
 221 number time steps is reached.

222 At the time of concentration  $t_c$ , the raindrops falling at the top of the catchment  
 223 arrives at the outlet, which means that the flow on the whole catchment has reached  
 224 an equilibrium state. After that, the whole catchment contributes to the runoff rate and  
 225 pollutant discharge at the outlet. At this equilibrium state, the runoff rate at the outlet

226 is equal to the rainfall input and the pollutant concentration is uniformly distributed  
 227 over the whole catchment. Then, the total water volume  $V_T$  on the whole catchment  
 228 has reached its maximum value and keeps unchanged, which can be derived by  
 229 making use of Eqs. (12), (15) and (16).

$$230 \quad V_T = \int_0^L Bh(x, t) dx = A \left( h_0 + \frac{5}{8} (IL/\alpha)^{3/5} \right) \quad (30)$$

231 During a tiny time interval of  $\Delta t$ , the volume of rainfall input to the whole  
 232 catchment can be calculated as:

$$233 \quad V_{rain} = BIL\Delta t \quad (31)$$

234 According to the conservation of mass of the solute, we can obtain the following  
 235 relationship from  $t$  to  $t + \Delta t$  ( $t_c \leq t$ ).

$$236 \quad C_t V_T = (C_t + \Delta C_t) (V_T + V_{rain}) \quad (32)$$

237 Combining Eqs. (30), (31) and (32) and neglecting the second-order small terms, the  
 238 above equation can be converted into a differential form:

$$239 \quad \frac{dC_t}{C_t} = - \frac{Idt}{h_0 + \frac{5}{8} (IL/\alpha)^{3/5}} \quad (33)$$

240 Integrating Eq. (33) and applying the initial condition yield:

$$241 \quad C_t = C_{t_c} e^{-I(t-t_c) / \left( h_0 + \frac{5}{8} (IL/\alpha)^{3/5} \right)} \quad (34)$$

242 Here,  $C_{t_c}$  is the solute concentration at  $t_c$ , which can be obtained using the  
 243 aforementioned modified Euler method.

244

## 245 **3 Model verification**

### 246 **3.1 Laboratory experiments**

247 To verify the model established in this study, a series of laboratory experiments  
248 were conducted in a rainfall-simulation hall. A large quantity of data was obtained in a  
249 relatively short period of time with the use of the rainfall simulator and a small  
250 idealized catchment. Details of the rainfall-simulation chamber can be found in  
251 previous studies (Xiao et al., 2017; Zhang et al., 2018). As mentioned before, this  
252 study focuses on the dissolved pollutant transport that accompanies the runoff flow  
253 over impervious surfaces. Similar to that in Xiao et al. (2017), a wooden board of 2.96  
254 m in length, 1.48 m in width and 0.02 m in thickness was used to represent the  
255 impervious surface. It should be noted that the wooden board used in this study is the  
256 same as the smooth board used in Xiao et al. (2017). The main reasons for choosing  
257 the wooden boards are: (a) they are light and easy to handle and (b) they are not easy  
258 to deform. As to the dimensions of wooden board, i.e. the length and width, they are  
259 determined by the size of steel flume (3 m × 1.5 m) that accommodates the board in  
260 the rain simulation hall. The steel flume that holds the board facilitates the adjustment  
261 of the catchment slope and the collection of runoff samples. The thickness of wooden  
262 board has no effect on the experimental results, as long as the wooden board's  
263 deformation is small in the experiment. As in the previous studies (Deng et al., 2005;  
264 Xiao et al., 2017; Zhang et al., 2018), sodium chloride (table salt) was chosen as the  
265 tracer to represent the pollutant. According to previous studies (Gao et al., 2004, 2005;

266 Deng et al., 2005; Kim et al., 2005; Egodawatta et al., 2007; Muthusamy et al., 2018)  
 267 over small catchments, the pollutant can usually be considered as uniformly  
 268 distributed. Hence, salt was uniformly spread on the catchment surface at the  
 269 beginning of each experiment. The total amount of table salt in each experiment was  
 270 fixed at 125 g. In contrast to the previous study (Xiao et al., 2017), a wider range of  
 271 slopes and rainfall intensities were tested in this study, as listed in Table 1. Each  
 272 rainfall event lasted for 28 minutes. For each experiment, the average rainfall intensity  
 273 was measured, as shown in Table 1. In Table 1, S0.5-1 refers to 0.5° slope, test case 1,  
 274 and similar convention applies to the names of the other test cases. The detailed  
 275 information about sample collection and data recording of the runoff water and  
 276 pollutant can be found in Xiao et al. (2017).

277 Table 1 Test cases and its measured rainfall intensity

Test case	<i>I</i> (mm/h)	Test case	<i>I</i> (mm/h)	Test case	<i>I</i> (mm/h)	Test case	<i>I</i> (mm/h)
S0.5-1	24.22	S1-7	138.96	S3-1	24.26	S4-4	79.29
S0.5-2	43.16	S2-1	20.76	S3-2	47.10	S4-5	106.93
S0.5-3	63.81	S2-2	41.72	S3-3	60.64	S4-6	117.52
S0.5-4	76.34	S2-3	62.61	S3-4	78.91	S4-7	146.61
S1-1	22.36	S2-4	83.99	S3-5	112.35	S5-1	41.92
S1-2	43.25	S2-5	99.63	S3-6	125.51	S5-2	80.75
S1-3	51.12	S2-6	110.59	S3-7	143.86	S5-3	119.83
S1-4	82.06	S2-7	119.92	S4-1	22.03	S6-1	46.61
S1-5	109.48	S2-8	139.91	S4-2	48.21	S6-2	87.76
S1-6	127.83	S2-9	149.75	S4-3	53.43	S6-3	131.55

278

### 279 3.2 Determination of parameters

280 Apart from the two parameters that define the test cases, i.e. the catchment slope  
281 and rainfall intensity, the depth of the control layer  $h_0$  and the Manning roughness  
282 coefficient  $n$  play important roles in our model. As the transport of dissolved  
283 pollutant is closely related to the overland flow process, an accurate quantification of  
284 the overland flow process is essential for predicting the transport of dissolved  
285 pollutant. According to Eq. (2) and Eq. (6), the parameters  $\alpha$  and  $n$  are  
286 interrelated and thus only one of them is needed for describing the rainfall-runoff  
287 process. Xiao et al. (2017) directly determined the value of  $\alpha$  for each slope by  
288 numerically fitting the initial rising limb of the runoff hydrograph using Eq. (2). The  
289 identical boards with the same slope took the same value of  $\alpha$ . According to Eq. (6),  
290 the values of  $n$  for different slopes can be obtained. Therefore, the values of  
291 Manning roughness coefficient  $n$  varied with the slope in their study. Xiao et al.  
292 (2017) noted that the variation may be due to the flow being not entirely hydraulically  
293 rough. From the available experimental data, it is difficult to judge whether such a  
294 conclusion is correct or not. The variation of  $n$  with the slope could also be  
295 attributed to the error in the experiment, as only a few data points were collected to  
296 plot the initial rising limb of the hydrograph, giving rise to large errors in the  
297 parameter regression. In the present study, we adopt the same value of  $n$  for all the  
298 experiments. By combining Eqs. (2) and (6), we can obtain:

$$299 \left( \frac{Q_t}{B\sqrt{S_0}} \right)^{3/5} / I = n^{-3/5} t \quad (35)$$

300 We define  $Q^* = \left( \frac{Q_t}{B\sqrt{S_0}} \right)^{3/5} / I$ . Hence,  $Q^*$  is proportional to  $t$  and this  
301 formulation applies to all the experiments. In order to reduce the error, we use all the  
302 experimental data about the initial rising limb of the hydrograph to determine the  
303 value of  $n$ . Fig. 1 shows the experimental results of  $Q^*$  for different test conditions.  
304 It is evident that  $Q^*$  for different conditions can be fitted well by the same linear  
305 relationship. It implies that taking the same value of  $n$  for all the experiments is  
306 reasonable. According to the linear regression, the value of Manning roughness  
307 coefficient  $n$  is determined to be 0.0457, which is very close to the average  
308 Manning roughness coefficient  $n$  of the smooth board (0.0477) in the study of Xiao  
309 et al. (2017). It indicates that the rainfall experiments have good accuracy and  
310 repeatability. This value of  $n$  obtained in this study might seem rather high if we  
311 consider that the recommended value in hydraulic manuals for a smooth wooden  
312 board surface is around 0.012 and 0.016. However, the extra roughness can be linked  
313 to the extremely small water depths in the experiments. The runoff in a thin layer is  
314 heavily affected by the effect of laminar flow in the viscous sublayer, which justifies  
315 the use of a higher bed friction coefficient. Hong et al (2016) also adopted a higher  
316 Manning coefficient value of 0.05 when reproducing the rainfall runoff process over a  
317 road surface. The time of concentration  $t_c$  for different rainfall events can be  
318 calculated using Eq. (1).



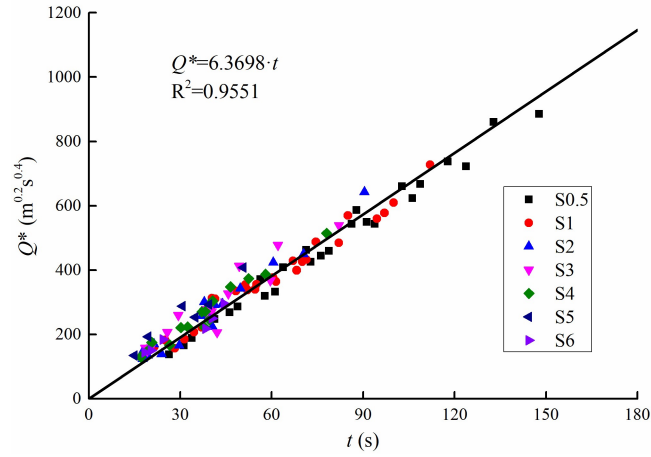


Figure 1.  $Q^*$  for different conditions

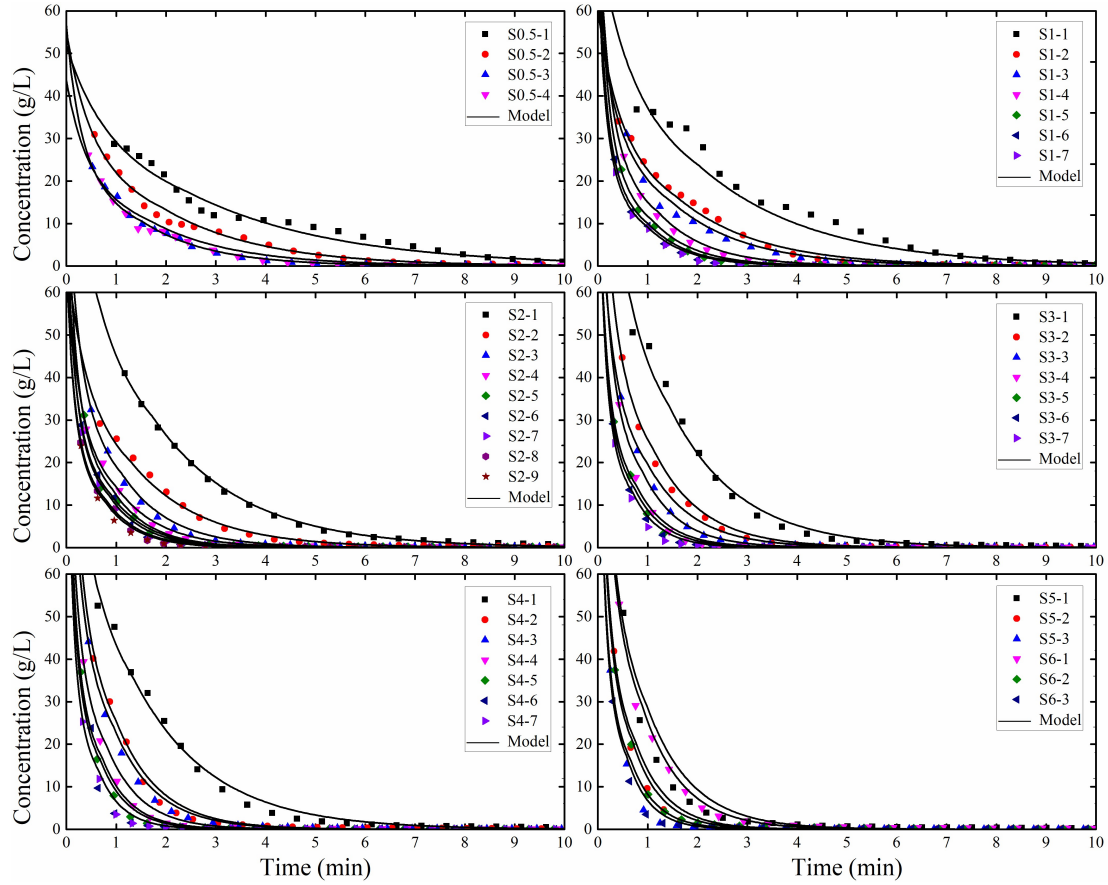
Up to this point, we have obtained the values of all free parameters except for the depth of control layer  $h_0$ . Unlike  $n$ , the value of  $h_0$  cannot be determined by direct data fitting. A more comprehensive least-square analysis is needed. The Nash-Sutcliffe efficiency ( $NSE$ ) (Nash and Sutcliffe, 1970) has often been adopted to evaluate the model performance. The formulation of  $NSE$  can be expressed as:

$$NSE = \mathbf{1} - \frac{\sum_t (Q_{o,t} - Q_{m,t})^2}{\sum_t (Q_{o,t} - \overline{Q_o})^2} \quad (36)$$

where  $Q_{o,t}$  is the observed value at time  $t$ ;  $Q_{m,t}$  is the modeled value at time  $t$ ;  $\overline{Q_o}$  is the average value of the observed data. Higher value of  $NSE$  represents a more accurate model. In this study, a Fortran program was written to determine the value of  $h_0$  in each experiment. In the Fortran program, the value of  $h_0$  is changed from 0.01 mm to 1.0 mm with depth step of 0.01 mm. At the end, the result with the largest  $NSE$  was selected. Therefore, the value of  $h_0$  for each experiment can be determined independently.

### 335 **3.3 Comparison of modeled and measured concentrations**

336 Pollutant concentration is one of the most important indicators for controlling the  
337 water quality. In this study, the pollutant concentration is therefore used to determine  
338 the value of  $h_0$  for each experiment by maximizing the Nash-Sutcliffe efficiency  
339 ( $NSE$ ) of the prediction. With the selected value of  $h_0$ , the comparisons between  
340 measured and predicted pollutant concentrations in different test runs are shown in  
341 Fig. 2. In each condition, the concentration of pollutant is seen to decrease with time  
342 and finally approaches zero. In addition, the pollutant concentration is found to be  
343 affected by the rainfall intensity and the bed slope. The greater the rainfall intensity  
344 and slope, the faster is the decrease of the pollutant concentration, which is largely  
345 due to the change in the water runoff process. As described in the previous section,  
346 the pollutant concentration is closely related to the overland flow process. Overall, the  
347 pollutant concentration can be satisfactorily predicted by the proposed transport  
348 model.



349

350

Figure 2. Measured and modeled pollutant concentrations

351

352

353

354

355

356

357

358

359

360

As mentioned before, the value of  $h_0$  is determined in this study by fitting the experimental results of the pollutant transport. Then, the values of  $C_0$  and  $t_c$  in each condition can be calculated from Eq. (14) and Eq. (1), respectively. Table 2 lists the estimated values of  $h_0$ ,  $NSE$ ,  $C_0$  and  $t_c$  for different rainfall events. It is obvious that all the values of  $NSE$  in different conditions are very close to 1, which reaffirms the good performance of the present transport model. Fig. 3 presents the variation of  $h_0$  in different conditions. It shows that there is no significant and consistent difference in  $h_0$  among the rainfall intensities. To prove the above point, the Pearson's correlation analysis between  $h_0$  and  $I$  was carried out using the SPSS statistical software (Version 25.0), and the results are presented in Table 3. It

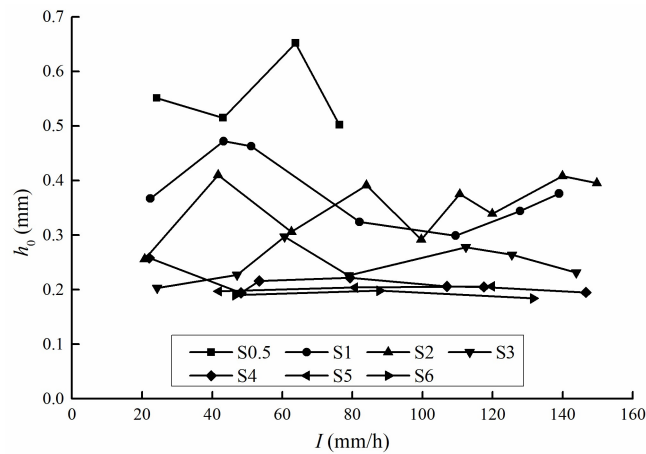
361 indicates that the value of  $h_0$  shows no significant correction with the rainfall  
362 intensity. In fact, the value of  $h_0$  for a given slope fluctuates within a small range  
363 over various rainfall intensity. Hence, it can be regarded that the value of  $h_0$  is a  
364 constant for a given slope. Taking series S2 for example, which has been subject to  
365 many rainfall intensities, Fig. 4 illustrates the variation of  $NSE$  with different  $h_0$ . In  
366 Fig. 4, the dotted vertical line represents the average value of  $h_0$  for different rainfall  
367 intensities. Taking the average value of  $h_0$  as the depth of the control layer for  
368 different rainfall intensities has little effect on the performance of the transport model.  
369 It implies that the above assumption is reasonable. Figure 5 shows the average values  
370 of  $h_0$  for different slopes. The value of  $h_0$  decreases with the increasing slope,  
371 indicating that an increased slope can accelerate the generation of the overland flow. It  
372 may be related to the surface tension or the normal water depth along the slope. A  
373 larger slope reduces the normal water depth, and thus the water holding capacity of  
374 the catchment. In addition, the value of  $h_0$  tends to be a constant at sufficiently large  
375 slopes. It indicates that a catchment has a limiting minimum water holding capacity,  
376 although the component of gravity along the slope keeps increasing with higher  
377 slopes.

378 Table 2 Estimated values of parameters for different test conditions

Test case	$h_0$ (mm)	$NSE$	$C_0$ (g/L)	$t_c$ (min)	Test case	$h_0$ (mm)	$NSE$	$C_0$ (g/L)	$t_c$ (min)
S0.5-1	0.551	0.9842	51.79	2.438	S3-1	0.203	0.9878	140.56	1.423
S0.5-2	0.515	0.9909	55.41	1.935	S3-2	0.227	0.9938	125.70	1.091
S0.5-3	0.652	0.9817	43.76	1.655	S3-3	0.297	0.9742	96.07	0.986
S0.5-4	0.502	0.9944	56.84	1.540	S3-4	0.226	0.9323	126.25	0.888

S1-1	0.367	0.9693	77.75	2.045	S3-5	0.278	0.9806	102.64	0.771
S1-2	0.472	0.9936	60.45	1.570	S3-6	0.264	0.9795	108.08	0.737
S1-3	0.463	0.9829	61.63	1.469	S3-7	0.231	0.9761	123.52	0.698
S1-4	0.324	0.9935	88.07	1.216	S4-1	0.258	0.9918	110.60	1.356
S1-5	0.299	0.9909	95.43	1.083	S4-2	0.194	0.9885	147.08	0.992
S1-6	0.344	0.9884	82.95	1.018	S4-3	0.216	0.9919	132.10	0.952
S1-7	0.376	0.9919	75.89	0.985	S4-4	0.222	0.9803	128.53	0.813
S2-1	0.256	0.9983	111.46	1.711	S4-5	0.206	0.9789	138.51	0.721
S2-2	0.410	0.9928	69.59	1.294	S4-6	0.205	0.8188	139.19	0.694
S2-3	0.306	0.9937	93.25	1.100	S4-7	0.195	0.9762	146.33	0.636
S2-4	0.391	0.9954	72.98	0.978	S5-1	0.197	0.9398	144.84	0.981
S2-5	0.292	0.9831	97.72	0.914	S5-2	0.204	0.9697	139.87	0.754
S2-6	0.375	0.9875	76.09	0.876	S5-3	0.206	0.9662	138.51	0.644
S2-7	0.339	0.9906	84.17	0.848	S6-1	0.190	0.9929	150.18	0.889
S2-8	0.408	0.9922	69.94	0.798	S6-2	0.198	0.9854	144.11	0.691
S2-9	0.395	0.9876	72.24	0.776	S6-3	0.184	0.9669	155.07	0.587

379



380

381

Figure 3. Estimated values of  $h_0$  for various conditions

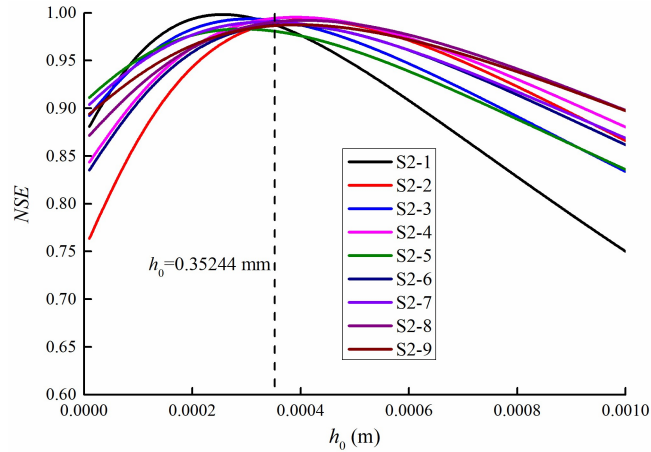
382

Table 3 Pearson's correlation coefficients for correlation between  $h_0$  and  $I$

Test case	S0.5	S1	S2	S3	S4	S5	S6
Number of samples	4	7	9	7	7	3	3
Pearson's correlation	0.068	-0.528	0.492	0.331	-0.652	0.952	-0.443

coefficient

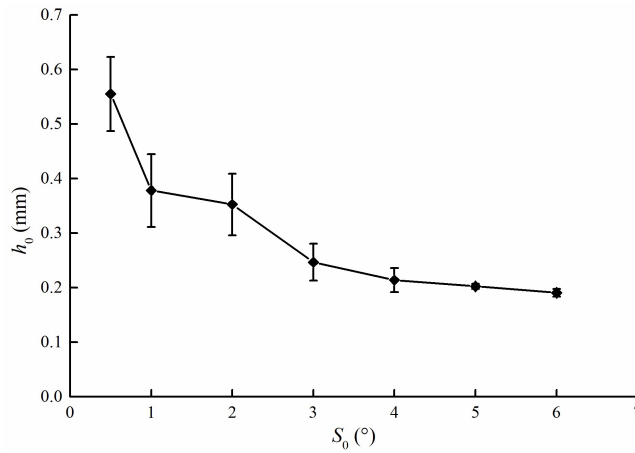
383 \*\*. Correlation is significant at the 0.01 level (2-tailed) \*. Correlation is significant at the 0.05  
384 level (2-tailed). According to Evans (1996), the range of absolute value of r is 0.00-0.19 “very  
385 weak”; 0.20-0.39 “weak”; 0.40-0.59 “moderate”; 0.60-0.79 “strong”; 0.80-1.0 “very strong”.



386

387

Figure 4. Variation of  $NSE$  for different  $h_0$



388

389

Figure 5. Average values of  $h_0$  for different slopes

### 390 3.4 Comparison between modeled and measured transport rates

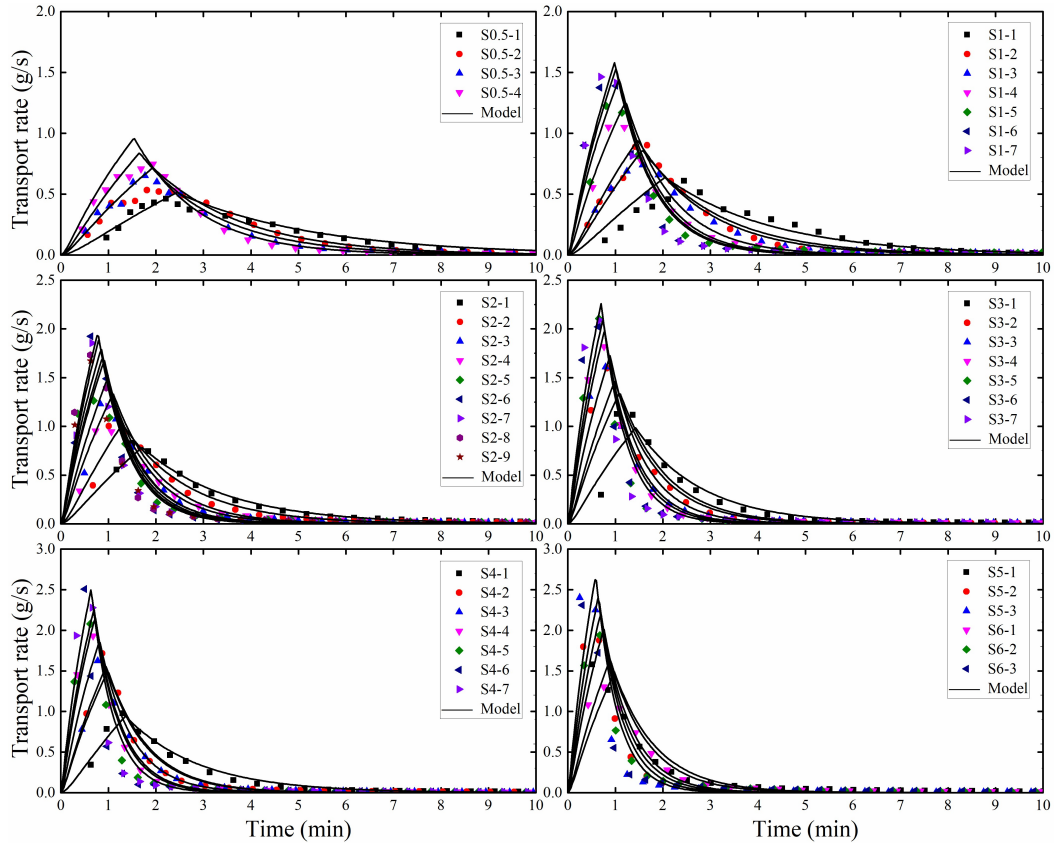
391 The pollutant transport rate is an important parameter, which can be defined as  
392 the flow rate of the pollutants transported out of the catchment. It can be calculated by  
393 the following equation:

$$394 M_t = C_t Q_t \quad (37)$$

395 where  $M_t$  is the pollutant transport rate at time  $t$  (g/s).

396 The observed and predicted pollutant transport rates under different conditions  
397 are shown in Fig. 6. Overall, the observed pollutant transport rates are in good  
398 agreement with those predicted by the transport model developed in this study. It is  
399 seen that the pollutant transport rates for different conditions show a similar  
400 single-peak shape, which consists of a steep-rising limb at the beginning and a  
401 sharp-falling limb later on. The pollutant transport rate increases from zero to a  
402 maximum and then decreases to zero. The larger the rainfall intensity and bed slope,  
403 the greater the maximum pollutant transport rate ( $M_{\max}$ ). This may be caused by the  
404 larger flow rate and water velocity associated with the larger rainfall intensity and bed  
405 slope. Figure 6 also shows that the present model can well predict the value of the  
406 maximum transport rate  $M_{\max}$ .

407 From the modeled results, the pollutant transport rate reaches a maximum at the  
408 time of concentration  $t_c$ , *i.e.* the end of the initial rising hydrograph period under an  
409 unceasing rainfall. It implies that the pollutant transport rate increases with the runoff  
410 rate during the initial runoff period, although the pollutant concentration decreases.  
411 Xiao et al. (2017) suggested that not all the maximum pollutant transport rates occur  
412 at the time of concentration  $t_c$ . However, the time of reaching the maximum value is  
413 very close to the time of concentration. This slight discrepancy may be related to the  
414 usage of a constant Manning roughness coefficient  $n$  for different slopes in this  
415 study, while different Manning roughness coefficients were obtained for different  
416 slopes in Xiao et al. (2017).



417

418 Figure 6. Measured and modeled pollutant transport rates

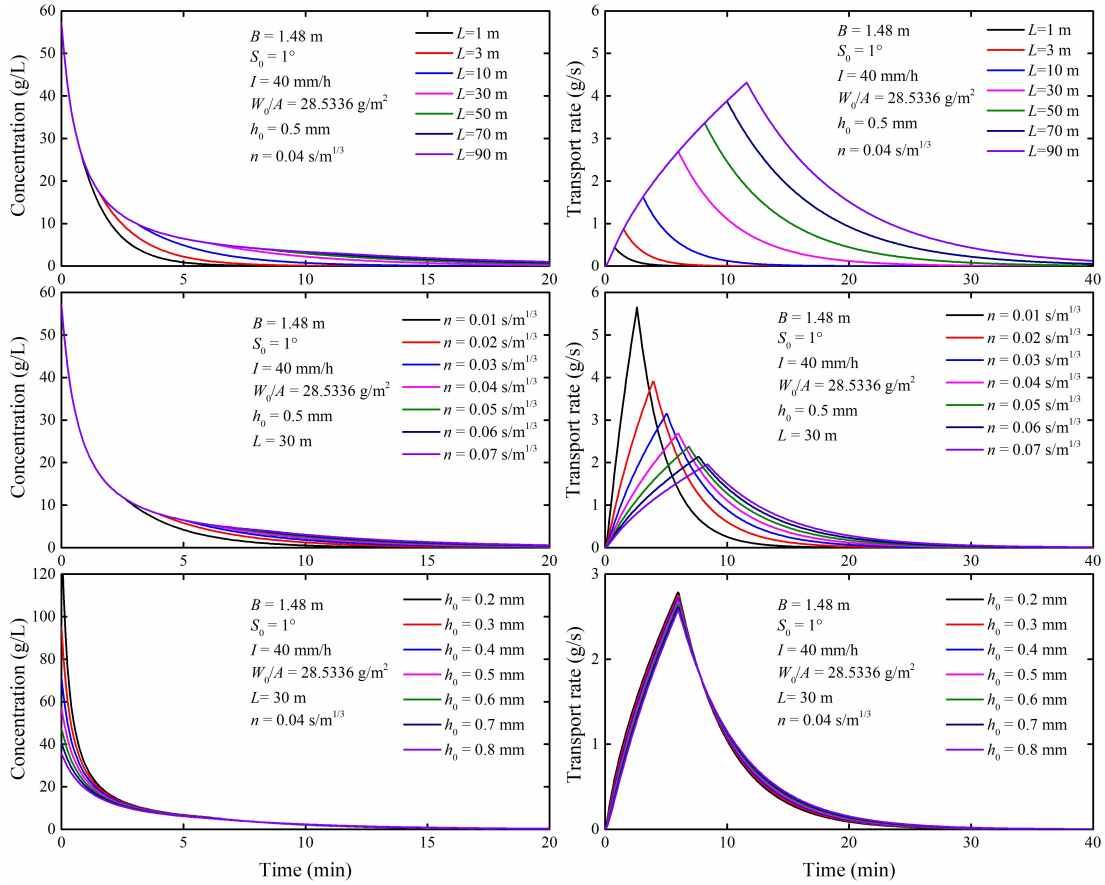
419 **3.5 Sensitivity analysis**

420 According to the developed transport model herein, it is expected that five  
 421 independent parameters ( $L$ ,  $h_0$ ,  $S_0$ ,  $n$  and  $I$ ) affect the pollutant transport  
 422 process. They all have clear physical meanings. Among these parameters,  $h_0$  and  $n$   
 423 were determined by fitting the experimental results in this study, while the other three  
 424 parameters were directly measured. Fig. 2 and Fig. 6 suggest that the rainfall intensity  
 425 and bed slope have huge impacts on the pollutant transport process, especially in the  
 426 initial phase. In addition, the pollutant transport process is particularly sensitive to  
 427 small rain intensity and bed slope.

428 To investigate the influence of the other three parameters ( $L$ ,  $h_0$  and  $n$ ), the  
 429 pollutant transport processes for various cases are modeled, as shown in Fig. 7. It



430 suggests that  $L$  and  $n$  exert significant effect on the pollutant concentration and  
431 transport rate, mainly in the middle period. Hence, the change in  $L$  and  $n$  will  
432 have great influence on the pollutant transport process. We can also see that a  
433 catchment with a short length leads to the faster transport of pollutant. Although the  
434 pollutant transport rate on a long catchment is large, it takes a longer time to reduce to  
435 zero. As for  $h_0$ , it shows that  $h_0$  has an impact on the concentration mainly in the  
436 initial runoff stage, and has little influence in the later stage. This is consistent with Eq.  
437 (14), from which it is clearly seen that  $h_0$  greatly influences the initial pollutant  
438 concentration. The difference in concentration will gradually diminish as the rainfall  
439 continues. In contrast, it is seen that  $h_0$  has no discernable effect on the pollutant  
440 transport rate due to the small runoff rate in the initial stage. Similar results can be  
441 found with vegetated surfaces (Zhang et al., 2018). Overall, as described before, the  
442 pollutant transport process is closely related to the water runoff process. As compared  
443 with  $h_0$ , the other parameters ( $S_0$ ,  $n$  and  $I$ ) have direct and significant influence  
444 on the runoff process. Therefore, these parameters exert significant influence on the  
445 pollutant transport process as well.



446

447

Figure 7. Pollutant concentrations and transport rates for various conditions

448

#### 4 Discussions

449

In the present investigation, a physically-based dissolved pollutant transport

450

model is proposed and verified. Xiao et al. (2017) also developed a semi-empirical

451

model to describe the dissolved pollutant transport process over impervious surfaces.

452

However, the main difference between the two models lies in the formulation of the

453

initial runoff stage. Xiao et al. (2017)'s model suggests that the pollutant

454

concentration conforms to an inverse S-curve, which is different from the model

455

presented in this study. Although the dissolved pollutant transport process can be

456

correctly described by both models, the model presented in this paper has some

457

advantages. Most importantly, the present model is physically based.

458 As mentioned before, the model developed herein adopts the idea of “stationary  
 459 water layer” proposed first by Zhang et al. (2018) for describing the solute transport  
 460 process over vegetated surface. In this paper, we define the thin water layer  
 461 underneath the overland flow as the “control layer”. The naming is mainly because  
 462 that the water flow over impervious surface cannot be totally stationary due to the  
 463 impact of rain drops. In contrast, vegetation can effectively reduce the impact of rain  
 464 drops. It is evident that runoff water and the water in the control layer will splash  
 465 under the impact of raindrops. From a statistical point of view, the amount of water  
 466 transported at any point on the catchment remains constant. Despite the water  
 467 exchange between the control layer and the overflow runoff, the amount of water in  
 468 the control layer remains constant.

469 According to previous studies (Xiao et al., 2017), for a constant rainfall event  
 470 over impervious surfaces, the expression of the dissolved pollutant concentration at  
 471 the equilibrium stage can be:

$$472 \quad C_t = C_{t_c} e^{-kt(t-t_c)} \quad (38)$$

473 where  $k$  is the wash-off coefficient ( $\text{mm}^{-1}$ ). From Eqs. (34) and (38), it is obvious

474 that  $k$  equals to  $1/\left(h_0 + \frac{5}{8}(IL/\alpha)^{3/5}\right)$ , where the term  $\left(h_0 + \frac{5}{8}(IL/\alpha)^{3/5}\right)$

475 represents the average water depth of the catchment at the equilibrium stage (Eq. 30).

476 Therefore, the wash-off coefficient  $k$  now carries a physical meaning as the  
 477 reciprocal of the average water depth over the catchment at the equilibrium stage.

478 From the expression  $k = 1/\left(h_0 + \frac{5}{8}(IL/\alpha)^{3/5}\right)$ , the values of  $k$  for all the

479 experimented cases can be obtained, as shown in Fig. 8. They show that the value of  
 480  $k$  increases with the increasing bed slope and decreasing rainfall intensity. It also  
 481 implies that a smaller slope and larger rainfall intensity increase the water holding  
 482 capacity of the catchment. In this study,  $k$  varies from 0.56 to 1.78  $\text{mm}^{-1}$ , which is  
 483 very close to that obtained in the previous study, which varies from 0.63 to 1.93  $\text{mm}^{-1}$   
 484 in Xiao et al. (2017). For a constant rainfall event over uniform rectangular  
 485 impervious surfaces, a constant value for  $k$  has been used to describe the transport  
 486 process of particulate pollutant in previous studies (Sartor and Boyd, 1974;  
 487 Egodawatta et al., 2007, 2009; Muthusamy et al., 2018). As for dissolved pollutant in  
 488 this study, the value of  $k$  also keeps unchanged at the equilibrium runoff stage with  
 489 an expression as follows:

$$490 \quad k = \mathbf{1} / \left( h_0 + \frac{\mathbf{5}}{\mathbf{8}} (IL/\alpha)^{3/5} \right) = \mathbf{1} / (h_0 + \mathbf{0.625}It_c) \quad (39)$$

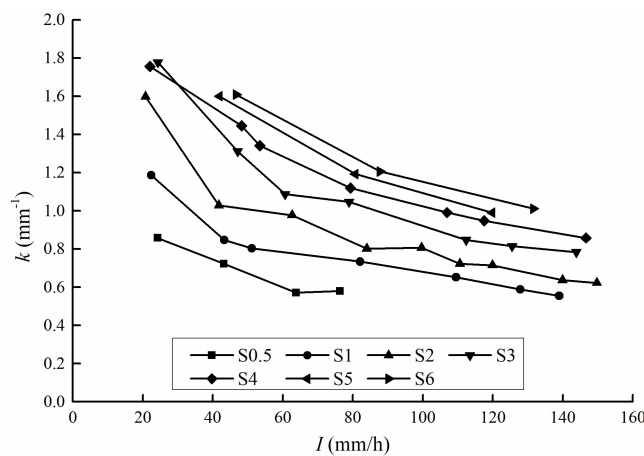
491 However, in the initial runoff stage ( $\mathbf{0} \leq t \leq t_c$ ), the value of  $k$  may vary with  
 492 time as the catchment has not completely reached the equilibrium stage. Here, the  
 493 wash-off coefficient  $k$  means the reciprocal of the average water depth over the  
 494 upstream part of the catchment where the equilibrium stage has already been  
 495 reached. The expression of  $k$  in the initial runoff stage can be easily obtained  
 496 from previous sections and Eq. (39):

$$497 \quad k = \mathbf{1} / (h_0 + \mathbf{0.625}It) \quad (40)$$

498 Figure 9 presents an example of the variation of  $k$  during a constant rainfall event.  
 499 It should be noted that the physical meaning of  $k$  may not be applicable to  
 500 particulate pollutants. After all, the transport mechanisms of dissolved and

501 particulate pollutants are different.

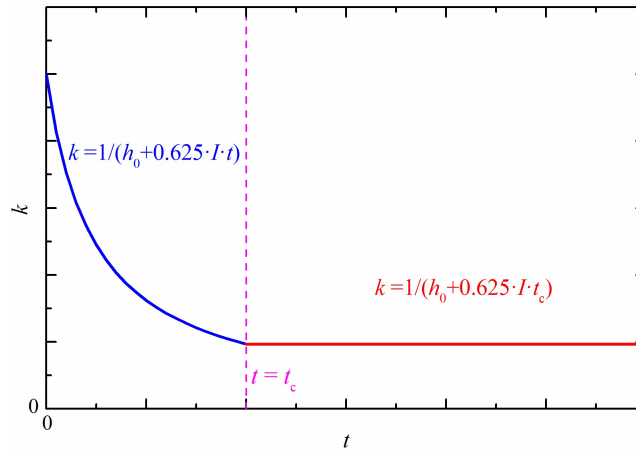
502 In summary, this study proposed a novel physically-based transport model for  
503 dissolved pollutant by adopting a “control layer” concept in overland flow. The  
504 model’s underlying assumptions are: (1) the rainfall intensity is uniformly  
505 distributed and does not change with time; (2) the catchment is a single slope with  
506 constant roughness; and (3) the pollutant is initially uniformly distributed over the  
507 catchment. The concept of “control layer” has been verified to be rational by a  
508 series of experiments, which helps advance our understanding of the mechanism of  
509 the dissolved pollutant transport. After extensive comparison with experimental  
510 results, the proposed model can be regarded to accurately reflect the physical  
511 processes for the dissolved pollutant transport over impervious surfaces. Although  
512 the model is restricted to idealized scenarios only in this study, it has the potential  
513 to become the building block to develop a distributed catchment model to simulate  
514 the response of a heterogeneous real-world catchment subject to spatially and  
515 temporally varied rainfall.



516

517

Figure 8. Values of  $k$  for various conditions



518

519 Figure 9. Values of  $k$  variation process during a constant rainfall event

520

## 521 **5 Conclusions**

522 This study developed a physically-based dissolved pollutant transport model

523 over impervious surfaces. This model adopts a key assumption that a thin water layer

524 named “control layer” is formed beneath the rapidly flowing water. The upper runoff

525 water is completely mixed with the water in the control layer at the same horizontal

526 position. To validate the proposed transport model, a series of simplified laboratory

527 experiments have been conducted in a rainfall simulation hall. The results show that

528 the pollutant concentration and pollutant transport rate can be accurately predicted by

529 the transport model proposed in this study. The maximum pollutant transport rate

530 takes place at the time of concentration, and is positively correlated with rainfall

531 intensity and the bed slope. The depth of the control layer mainly depends on the bed

532 slope and it has no noticeable dependence on the rainfall intensity. Sensitivity analysis

533 showed that rainfall intensity, bed slope, surface roughness and the length of

534 catchment are dominant factors in controlling the dissolved pollutant transport. In

535 contrast, the depth of the control layer mainly influences the initial pollutant  
536 concentration, but it has no significant effect on the pollutant transport rate. The  
537 wash-off coefficient  $k$  for the dissolved pollutant carries a physical meaning as the  
538 reciprocal of the average water depth in the catchment area over which the  
539 equilibrium stage has been reached. Therefore, it is related to the water holding  
540 capacity of the catchment.

541 Although the physical meaning of  $k$  for dissolved pollutant has been found,  
542 further study will be needed to confirm whether the same meaning holds for the  
543 particulate pollutant transport. A real-life urban area is much more complicated, with  
544 spatially and temporally varied ground features. A robust distributed hydrological and  
545 water quality model will be needed to take into account such complicated scenarios.

546

#### 547 **Conflict of interest**

548 The authors declare that there is no conflict of interests regarding the publication  
549 of this paper.

550

#### 551 **Acknowledgements**

552 This work was financially supported by the National Key Research and  
553 Development Program of China (2016YFC0402605), the Natural science foundation  
554 of Jiangsu province (BK20191299), the 111 Project (B17015), the Royal Academy of  
555 Engineering UK-China Urban Flooding Research Impact Programme

556 (UFRIP\100051) and the Special Fund of State Key Laboratory of Hydrology-Water  
557 Resources and Hydraulic Engineering(20195025712). The authors wish to thank  
558 Professor Bidya Sagar Pani of the Indian Institute of Technology-Bombay for  
559 providing valuable suggestions and language help.

560

## 561 **References**

562 Ahuja, L. R., Sharpley, A. N., Yamamoto, M., Menzel, R. G., 1981. The depth of  
563 rainfall-runoff-soil interaction as determined by 32P. Water Resources Research. 17(4),  
564 969-974.

565 Alley W.M., 1981. Estimation of impervious-area wash-off parameters. Water Resources Research.  
566 17: 1161-1166.

567 Angela Gorgoglione, Fabián A. Bombardelli, Bruno J.L. Pitton, Lorence R. Oki, Darren L. Haver,  
568 Thomas M. Young., 2019. Uncertainty in the parameterization of sediment build-up and  
569 wash-off processes in the simulation of sediment transport in urban areas. Environmental  
570 Modelling & Software. 111: 170-181.

571 Brezonik P.L., Stadelmann T.H., 2002. Analysis and predictive models of stormwater runoff  
572 volumes, loads, and pollutant concentrations from watersheds in the Twin Cities metropolitan  
573 area, Minnesota, USA. Water Research. 36: 1743-1757.

574 Charbeneau R.J., Barrett M.E., 1998. Evaluation of methods for estimating stormwater pollutant  
575 loads. Water Environment Federation. 70: 1295-1302.

576 Deletic A., Ashley R., Rest D., 2000. Modelling input of fine granular sediment into drainage  
577 systems via gully-pots. Water Research. 34: 3836-3844.



578 Deng Z., de Lima J.L.M.P., Singh V.P., 2005. Transport rate-based model for overland flow and  
579 solute transport: Parameter estimation and process simulation. *Journal of Hydrology*. 315:  
580 220-235.

581 Egodawatta P., Thomas E., Goonetilleke A., 2007. Mathematical interpretation of pollutant  
582 wash-off from urban road surfaces using simulated rainfall. *Water Research*. 41: 3025-3031.

583 Egodawatta P., Thomas E., Goonetilleke A., 2009. Understanding the physical processes of  
584 pollutant build-up and wash-off on roof surfaces. *Science of the total environment*. 407:  
585 1834-1841.

586 Evans, J.D., 1996. *Straightforward Statistics for the Behavioural Sciences*. Brooks/Cole Pub. Co.,  
587 Pacific Grove.

588 Fletcher T.D., Andrieu H., Hamel P., 2013. Understanding, management and modelling of urban  
589 hydrology and its consequences for receiving waters: a state of the art. *Advances in Water*  
590 *Resources*. 51: 261-279.

591 Gao B., Walter M.T., Steenhuis T.S., Hogarth W.L., Parlange J.Y., 2004. Rainfall induced chemical  
592 transport from soil to runoff: theory and experiments. *Journal of Hydrology*. 295(1-4):  
593 291-304.

594 Gao B., Walter M.T., Steenhuis T.S., Parlange J.Y., Richards B.K., Hogarth W.L., Rose C.W.,  
595 2005. Investigating raindrop effects on transport of sediment and non-sorbed chemicals from  
596 soil to surface runoff. *Journal of Hydrology*. 308: 313-320.

597 Gauta Jarrod, Chua Lloyd HC., Irvine Kim N., Le Song Ha., 2019. Modelling the washoff of  
598 pollutants in various forms from an urban catchment. *Journal of Environmental Management*.  
599 246: 374-383.

600 Goonetilleke A., Thomas E., Ginn S., Gilbert D., 2005. Understanding the role of land use in  
601 urban stormwater quality management. *Journal of Environmental Management*. 74: 31-42.

602 Hong Yi, Bonhomme Celine, Le Minh-Hoang, Chebbo Ghassan., 2016. A new approach of  
603 monitoring and physically-based modelling to investigate urban wash-off process on a road  
604 catchment near Paris. *Water Research*. 102: 96-108.

605 Hong Yi, Bonhomme Celine, Bout Bastian Van den, Jetten Victor, Chebbo Ghassan.,2017.  
606 Integrating atmospheric deposition, soil erosion and sewer transport models to assess the  
607 transfer of traffic-related pollutants in urban areas. *Environmental Modelling & Software*. 96:  
608 158-171.

609 Irish L.B., Barrett M.E., Malina J.F., Charbeneau R.J., 1998. Use of regression models for  
610 analyzing highway storm-water loads. *Journal of Environmental Engineering*. 124: 987-993.

611 Kim L., Kayhanian M., Zoh K., Stenstrom M.K., 2005. Modeling of highway stormwater runoff.  
612 *Science of the Total Environment*. 348: 1-18.

613 Lee J.H., Bang K.W., 2000. Characterization of urban stormwater runoff. *Water Research*. 34:  
614 1773-1780.

615 Liang D.F., Özgen I., Hinkelmann R., Xiao Y., Chen J.M., 2015. Shallow water simulation of  
616 overland flows in idealised catchments. *Environmental Earth Sciences*. 74: 7307-7318.

617 Massoudieh A., Abrishamchi A., Kayhanian M., 2008. Mathematical modeling of first flush in  
618 highway storm runoff using genetic algorithm. *Science of the total environment*. 398:  
619 107-121.

620 Metcalf, Eddy Inc., 1971. Storm Water Management Model, volume 1: final report,  
621 Environmental Protection Agency. Washington, D.C.

622 Montgomery, M.R., 2008. The urban transformation of the developing world. *Science*. 319:  
623 761-764.

624 Miguntanna Nandika P., Liu An, Egodawatta Prasanna, Goonetilleke Ashantha, 2013.  
625 Characterising nutrients wash-off for effective urban stormwater treatment design. *Journal of*  
626 *Environmental Management*. 120: 61-67.

627 Millar R.G., 1999. Analytical determination of pollutant wash-off parameters. *Journal of*  
628 *Environmental Engineering*. 125: 989-992.

629 Muthusamy Manoranjan, Tait Simon, Schellart Alma, Beg Md Nazmul Azim, Carvalho Rita F., de  
630 Lima João L.M.P., 2018. Improving understanding of the underlying physical process of  
631 sediment wash-off from urban road surfaces. *Journal of Hydrology*. 557: 426-433.

632 Nash J.E., Sutcliffe J.V., 1970. River flow forecasting through conceptual models part I — A  
633 discussion of principles. *Journal of Hydrology*. 10: 282-290.

634 Osuch-Pajdzińska E., Zawilski M., 1998. Model of storm sewer discharge: I Description. *Journal*  
635 *of Environmental Engineering*. 124: 593-599.

636 Sartor J.D., Boyd G.B., Agardy F.J., 1974. Water pollution aspects of street surface contaminants.  
637 *Journal-Water Pollution Control Federation*. 46(3): 458.

638 Shaw S.B., Walter M.T., Steenhuis T.S., 2006. A physical model of particulate washoff from rough  
639 impervious surfaces. *Journal of Hydrology*, 2006, 327: 618-626.

640 Sheng Y., Ying G., Sansalone J., 2008. Differentiation of transport for particulate and dissolved  
641 water chemistry load indices in rainfall–runoff from urban source area watersheds. *Journal of*  
642 *Hydrology*. 361: 144-158.

643 Soonthornnonda Puripus, Christensen Erik R., Liu Yang, Li Jin., 2008. A washoff model for

644 stormwater pollutants. *Science of the Total Environment*. 402: 248-256.

645 Stephenson D., Meadows M.E., 1986. *Kinematic Hydrology and Modelling*. Elsevier Science  
646 Pubfishers. New York, USA.

647 Vaze J., Chiew F.H.S., 2002. Experimental study of pollutant accumulation on an urban road  
648 surface. *Urban Water*. 4: 379-389.

649 Wang S.M., He Q., Ai H.N., Wang Z.T., Zhang Q.Q., 2013. Pollutant concentrations and pollution  
650 loads in stormwater runoff from different land uses in Chongqing. *Journal of Environmental  
651 Sciences*. 25: 502-510.

652 Xiao Yang, Zhang Taotao, Liang Dongfang, Jack M. Chen., 2016. Experimental study of water  
653 and dissolved pollutant runoffs on impervious surfaces. *Journal of hydrodynamics*. 28(1):  
654 162-165.

655 Xiao Yang, Zhang Taotao, Wang Lei, Liang Dongfang, Xu Xingwu., 2017. Analytical and  
656 experimental study on dissolved pollutant wash-off over impervious surfaces. *Hydrological  
657 Processes*. 31(25): 4520-4529.

658 Zhang Taotao, Xiao Yang, Liang Dongfang, Wang Lei., 2018. Experimental and analytical studies  
659 of solute transport during run-off over vegetated surfaces. *Hydrological Processes*. 32(15):  
660 2335-2345.

661